Spacecraft attitude and rate estimation and control using the SDRE method

Daniel Choukroun[1] *and Ozan Tekinalp*[2]

[1]*Delft University of Technology, Faculty of Aerospace Engineering*
Kluyverweg 1, 2627 HS, Delft, The Netherlands

[2]*Middle East Technical University, Aerospace Engineering Department*
Dumlupinar Bulvari 1, 06800 Ankara, Turkey

d.choukroun@tudelft.nl, tekinalp@metu.tr

Abstract

This work investigates the performances of several State-Dependent Riccati Equation algorithms for the estimation and control of attitude and attitude rates of a rigid-body spacecraft. The estimators are designed to process line-of-sight and gyros measurements corrupted by white noises and potentially drifting biases. The case of gyroless estimation is also addressed. The vector measurements are linear-in-quaternion with state-dependent white noises. The controllers implement single-loop and dual-loop approaches. Under equivalent conditions, the single-loop controller outperforms the dual-loop controller wether by requiring less control energy or by having a quicker pointing transient. The dual-loop approach however requires less computations and shows a less aggressive control transient. Estimation performances are the limiting factor in the proposed partial information closed-loop attitude and rate controllers. With angular deviations in the vector observations of 0.5 deg, with or without gyros, and neglecting perturbations, pointing performance levels of typically 0.1 deg are demonstrated via numerical simulations.

1. Introduction

In any spacecraft mission, the task of attitude determination and control is critical for success [1]. Among the many methodologies from the realm of nonlinear optimal filtering and control, the State-Dependent Riccati Equation (SDRE) method has received increased attention [2, 3], in particular due to its application to the field of spacecraft attitude estimation and control. Reference [4] shows that SDRE control techniques provide effective performances for spacecraft (S/C) orientation stability using reaction wheel torques and modeling the S/C momentum, the wheels momentum, the angular rates and the quaternion as states. In [5] the SDRE approach was applied to a control problem for relative attitude and attitude rate, augmented with relative position and velocity, between a tumbling target S/C and a chaser S/C. The results show desirable responses for a wide range of target attitude motions. The scope of these works however were limited to full state information. An application of SDRE filtering to rate estimation, and a variation called pseudolinear Kalman filter (PSELIKA), was presented in [6] based on the differentiation of line-of-sight (LOS) measurements. The proposed filters were successfully applied to real data yet under the assumption of perfect attitude information and with no biases in the measurements. These results were extended to the problem of attitude and attitude rate estimation with measurements biases in [7]. Line-of-sight vector and full quaternion measurement were considered along with the two parameterizations, quaternion and the rotation matrix, when developing the SDRE filters. The underlying assumption to obtain a linear quaternion measurement was the availability of a star tracker on-board. Reference [8] introduces an integrated attitude determination and control algorithm based on magnetic measurements and actuation. The quaternion and the rates are controlled via a modified SDRE controller using estimated values. The filter is designed to estimate a magnetic dipole residual and a drag coefficient in addition to the attitude and rates. The simulated results demonstrate satisfactory estimation and pointing accuracy. Within the scope of [8] however, the LOS measurements did not include biases, the filter was a standard extended Kalman filter. Reference [9] includes results showing that the PSELIKA filter [7] seems more robust than a standard EKF to initial errors. It also introduces an optimized SDRE technique, and applies it to enhance S/C rate control with full information, but falls short from

combining estimation and control. Combined SDRE estimation and control is applied in [10] to the problem of orbital and attitude control of spacecraft in formation flying. The proposed approach seems affective and emphasizes the measurement timing strategy. However, the control architecture in [10], as in [4, 5, 8], assumes a single-loop feedback while advantages exist in designing a multiple-loops architecture [13, 14].

This work is concerned with the development of several combined SDRE estimation and control algorithms for S/C attitude and rates with and without gyro measurements and using vector observations. The contributions of the work are two folds: 1) it implements a single-loop and a dual-loop architecture for the control and investigates their relative advantages via extensive simulations, 2) the filters' designs implement a pseudolinear quaternion measurement model introduced previously in [11] which alleviates the need for star-tracker on-board. The investigation is systematically performed considering the control problem with full information, the estimation problem without control with various measurement models, and the combined case. The sensors models include white noises and drifting biases that are typical for S/C systems. Comparative simulations are performed showing the effectiveness of the approach attitude estimation and stabilization. The relative loss in performance due to the dual-loop approach seems acceptable. The major performance differences occur between the gyroless and gyro-based controllers: the former are quicker to converge but has go a relatively noisy steady-state while the latter shows a delay in the rate estimation but settles on a smoother steady-state regime.

Section 2 includes a background on the SDRE estimation and control approaches. Secion 3 presents the single-loop and dual-loop controllers for attitude and rate control with full information. Section 4is concerned with the quaternion and rates estimation problem for various sensors' and dynamics models. Section 5 addresses the combined estimation and control implementation. Section 6 presents the conclusions.

2. Background

2.1 SDRE nonlinear control

This section follows the exposition in [2]. Consider the nonlinear dynamical system described by the following differential equations

$$\dot{\mathbf{x}} = a(\mathbf{x}) + B(\mathbf{x})\mathbf{u} \tag{1}$$

where $\mathbf{x} \in \mathbb{R}^n$ is the state, $\mathbf{u} \in \mathbb{R}^m$ is the control, $a(\mathbf{x}) \in C^l$, $B(x) \in C^l$, for $l \geq 1$. It is assumed that $a(0) = 0$ and $B(\mathbf{x}) \neq 0$ for all $\mathbf{x}$. The nonlinear regulator problem is formulated as follows: Minimize

$$J = \frac{1}{2}\int_0^\infty \mathbf{x}^T Q(\mathbf{x})\mathbf{x} + \mathbf{u}^T R(\mathbf{x})\mathbf{u}\, dt \tag{2}$$

where $Q(\mathbf{x}) \geq 0$ and $R(\mathbf{x}) > 0$ for all $\mathbf{x}$, with respect to the control $\mathbf{u}$ under the dynamical constraint (1). That constraint can be represented by the following linear structure with state-dependent coefficients (SDC):

$$\dot{\mathbf{x}} = A(\mathbf{x})\mathbf{x} + B(\mathbf{x})\mathbf{u} \tag{3}$$

The SDRE approach of obtaining a suboptimal solution of problem (1)-(2) is described by the following algorithm:

$$A^T(\mathbf{x})P + PA(\mathbf{x}) - PB(\mathbf{x})R^{-1}(\mathbf{x})B^T(\mathbf{x})P + Q(\mathbf{x}) = 0 \mapsto P(\mathbf{x}) \geq 0 \tag{4}$$

$$K(\mathbf{x}) = R^{-1}(\mathbf{x})B^T(\mathbf{x})P(\mathbf{x}) \tag{5}$$

$$\mathbf{u} = -K(\mathbf{x})\mathbf{x} \tag{6}$$

2.2 SDRE nonlinear filtering

This section is based on [6]. Given the following nonlinear state-space plant,

$$\dot{\mathbf{x}} = f(\mathbf{x}) + G(\mathbf{x})\,\mathbf{w} \tag{7}$$

$$\mathbf{z}_{_k} = h(\mathbf{x}_{_k}) + \Gamma(\mathbf{x}_{_k})\mathbf{v}_{_k} \tag{8}$$

where $\mathbf{x}$ denotes the state vector at time t, $\mathbf{w}$ and $\mathbf{v}_k$ are zero-mean white noise processes with known intensity and covariance matrices, W and V_k, respectively, and given their associated SDC expressions, i.e.

$$f(\mathbf{x}) = F(\mathbf{x})\mathbf{x} \tag{9}$$
$$h(\mathbf{x}_k) = H(\mathbf{x}_k)\mathbf{x}_k \tag{10}$$

then the SDRE filter is summarized as follows in a continuous-discrete form.

2.2.1 Time propagation stage

$$\dot{\hat{\mathbf{x}}} = f(\hat{\mathbf{x}}) \tag{11}$$
$$\dot{P} = F(\hat{\mathbf{x}})P + PF^T(\hat{\mathbf{x}}) + G(\hat{\mathbf{x}})WG^T(\hat{\mathbf{x}}) \tag{12}$$

with initial conditions $\hat{\mathbf{x}}_{k/k}$, $P_{k/k}$. The vector $\hat{\mathbf{x}}$ denotes the estimate at t given the measurements until t_k, where $t_k \leq t \leq t_{k+1}$, and P denotes the approximate covariance matrix of the associated estimation error.

2.2.2 Measurement update stage

$$S_{k+1} = H(\hat{\mathbf{x}}_{k+1/k})\, P_{k+1/k} H^T(\hat{\mathbf{x}}_{k+1/k}) + \Gamma(\hat{\mathbf{x}}_{k+1/k})\, V_{k+1} \Gamma^T(\hat{\mathbf{x}}_{k+1/k}) \tag{13}$$
$$K_{k+1} = P_{k+1/k} H^T(\hat{\mathbf{x}}_{k+1/k})\, S_{k+1}^{-1} \tag{14}$$
$$\hat{\mathbf{x}}_{k+1/k+1} = \left[I - K_{k+1} H(\hat{\mathbf{x}}_{k+1/k})\right] \hat{\mathbf{x}}_{k+1/k} + K_{k+1}\mathbf{z}_{k+1} \tag{15}$$
$$P_{k+1/k+1} = \left[I - K_{k+1} H(\hat{\mathbf{x}}_{k+1/k})\right]\, P_{k/k}\, \left[I - K_{k+1} H(\hat{\mathbf{x}}_{k+1/k})\right]^T + K_{k+1}\Gamma(\hat{\mathbf{x}}_{k+1/k})\, V_{k+1} \Gamma^T(\hat{\mathbf{x}}_{k+1/k}) K_{k+1}^T \tag{16}$$

3. Attitude control with full information

Consider a fully actuated rigid-body spacecraft (S/C) in rotation with respect to an inertial Cartesian coordinates frame $\mathcal{I}$. Let $\mathcal{B}$ denote a Cartesian coordinates body-frame, $\mathbf{q}$ denote the quaternion of rotation from $\mathcal{B}$ to $\mathcal{I}$, $\boldsymbol{\omega}$ denote the angular rate vector of $\mathcal{B}$ with respect to $\mathcal{I}$ resolved in $\mathcal{B}$. Neglecting non-control torques, the S/C kinematics and dynamics are governed by the following differential equations:

$$\dot{\boldsymbol{\omega}} = -J^{-1}\left[\boldsymbol{\omega}\times\right] J\boldsymbol{\omega} + J^{-1}\mathbf{u} \tag{17}$$
$$\dot{\mathbf{q}} = \frac{1}{2}\,\Xi(\mathbf{q})\boldsymbol{\omega} \tag{18}$$

where J denotes the S/C tensor of inertia expressed in $\mathcal{B}$, $\mathbf{u}$ is the control torque vector, $\Xi(\mathbf{q})$ is defined as follows

$$\Xi(\mathbf{q}) = \begin{bmatrix} [\mathbf{e}\times] + q\, I_3 \\ -\mathbf{e}^T \end{bmatrix} \tag{19}$$

and $\mathbf{e}, q$ denote the vector and the scalar part of $\mathbf{q}$, respectively. The matrices $[\mathbf{a}\times]$ in Eqs.(17) and (19) are defined as follows for any 3×1 vector $\mathbf{a}$:

$$[\mathbf{a}\times] = \begin{bmatrix} 0 & -a(3) & a(2) \\ a(3) & 0 & -a(1) \\ -a(2) & a(1) & 0 \end{bmatrix} \tag{20}$$

3.1 Single-loop controller

3.1.1 Model and problem formulation

Since the quaternion of rotation $\mathbf{q}$ is constrained to be a unit-norm vector in $\mathbb{R}^4$, the scalar part can be expressed as a function of the vector part, i.e.

$$q = \sqrt{1 - \mathbf{e}^T\mathbf{e}} \tag{21}$$

Notice that the positive square-root is chosen here without loss of generality since the quaternions $\mathbf{q}$ and $(-\mathbf{q})$ represent the same rotation. Inserting Eq. (21) into Eq. (18) and discarding the equation in q yields the following state-dependent coefficient (SDC) model for the augmented state $(\boldsymbol{\omega},\mathbf{e})$:

$$\begin{bmatrix}\dot{\boldsymbol{\omega}}\\ \dot{\mathbf{e}}\end{bmatrix} = \begin{bmatrix} -J^{-1}\left[\boldsymbol{\omega}\times\right]J & O_3 \\ \frac{1}{2}\left(\left[\mathbf{e}\times\right]+\sqrt{1-\mathbf{e}^T\mathbf{e}}\,I_3\right) & O_3\end{bmatrix}\begin{bmatrix}\boldsymbol{\omega}\\ \mathbf{e}\end{bmatrix} + \begin{bmatrix}J^{-1}\\ O_3\end{bmatrix}\mathbf{u} \tag{22}$$

Notice that the (21) submatrix in Eq. (22) is non-singular for any $\mathbf{e}$ except when $\mathbf{e}$ is a unit-norm vector, i.e., when the Euler angle of rotation is 180^o. Since the attitude representation was reduced to three parameters, this singularity is expected. As a result, the proposed model lacks pointwise controllability at these particular points. In this work, initial angular deviations less than 180^o are considered.
The proposed single-loop SDRE attitude controller is a suboptimal solution to the following quadratic integral cost minimization problem:

$$\min_{\mathbf{u}}\left\{\int_0^\infty \mathbf{x}^T Q\mathbf{x}+\mathbf{u}^T R\mathbf{u}\,dt\right\} \tag{23}$$

where $\mathbf{x}=(\boldsymbol{\omega},\mathbf{e})$, subject to Eq. (22), Q is a 6×6 positive semi-definite matrix and R is a 3×3 positive definite matrix.

3.1.2 Algorithm summary

Given $\boldsymbol{\omega},\mathbf{e}$, the single-loop SDRE control is computed as follows:

$$A = \begin{bmatrix} -J^{-1}\left[\boldsymbol{\omega}\times\right]J & O_3 \\ \frac{1}{2}\left(\left[\mathbf{e}\times\right]+\sqrt{1-\mathbf{e}^T\mathbf{e}}\,I_3\right) & O_3\end{bmatrix} \tag{24}$$

$$B = \begin{bmatrix}J^{-1}\\ O_3\end{bmatrix} \tag{25}$$

$$A^TP+PA+Q-PBR^{-1}B^TP=O_6 \mapsto P>0 \tag{26}$$

$$K = R^{-1}B^TP \tag{27}$$

$$\mathbf{u} = -K\begin{bmatrix}\boldsymbol{\omega}\\ \mathbf{e}\end{bmatrix} \tag{28}$$

Notice that the SDARE (26) that needs to be solved for the positive definite matrix P is a 6×6 matrix equation. The matrix P is ensured to exist except for $\mathbf{e}^T\mathbf{e}=1$. The (suboptimal) control $\mathbf{u}$ from Eq. (28) is implemented in Eq. (17) in order to drive the system to rest such that $\mathcal{B}$ coincides with $\mathcal{I}$.

3.2 Dual-Loop controller

The dual-loop controller approach exploits the cascaded property of the S/C dynamical equations (17)(18) where $\mathbf{u}$ drives the dynamics of $\boldsymbol{\omega}$, which itself drives the dynamics of $\mathbf{q}$. Henceforth two cascaded optimal control problems are formulated yielding two cascaded controllers in a dual-loop configuration.

3.2.1 Model and problem formulation

For convenience, the dynamical equation for $\mathbf{e}$ is rewritten as follows:

$$\dot{\mathbf{e}} = \frac{1}{2}\left(\left[\mathbf{e}\times\right]+\sqrt{1-\mathbf{e}^T\mathbf{e}}\,I_3\right)\boldsymbol{\omega} \tag{29}$$

Equation (29) appears as an SDC model equation for the state $\mathbf{e}$ with the angular rate vector as input and a state-dependent input gain matrix. The solution of the associated SDRE regulator problem, which is expressed as

$$\min_{\boldsymbol{\omega}}\left\{\int_0^\infty \mathbf{e}^T Q_o\mathbf{e}+\boldsymbol{\omega}^T R_o\,\boldsymbol{\omega}dt\right\} \tag{30}$$

subject to Eq. (29), where $Q_o\geq O_3, R_o > O_3$ (subscript $_o$ stands for 'outer-loop'), will thus provide a command trajectory for the angular rate vector. Let $\boldsymbol{\omega}_c$ denote the command (desired) trajectory for $\boldsymbol{\omega}$ generated by the SDRE solution of problem (30). The second control problem is then a tracking problem formulated as follows:

$$\min_{\mathbf{u}}\left\{\int_0^\infty (\boldsymbol{\omega}-\boldsymbol{\omega}_c)^T Q_i(\boldsymbol{\omega}-\boldsymbol{\omega}_c)+\mathbf{u}^T R_i\mathbf{u}\,dt\right\} \tag{31}$$

subject to the dynamical equation for $\boldsymbol{\omega}$, i.e.,

$$\dot{\boldsymbol{\omega}} = -\left(J^{-1}\left[\boldsymbol{\omega}\times\right]J\right)\boldsymbol{\omega} + J^{-1}\mathbf{u} \tag{32}$$

where $Q_i \geq O_3, R_i > O_3$, (subscript $_i$ stands for 'inner-loop'). Clearly, Eq. (32) provides an SDC model equation for the dynamics of $\boldsymbol{\omega}$, and the SDRE solution is readily obtained from the linear quadratic tracking theory.

3.2.2 Algorithm summary

Given $\boldsymbol{\omega}$,$\mathbf{e}$, compute:

$$B_o = \frac{1}{2}\left([\mathbf{e}\times] + \sqrt{1-\mathbf{e}^T\mathbf{e}}\, I_3\right) \tag{33}$$

$$Q_o - P_o B_o R_o^{-1} B_o^T P_o = O_3 \mapsto P_o > 0 \tag{34}$$

$$K_o = R_o^{-1} B_o^T P_o \tag{35}$$

$$\boldsymbol{\omega}_c = -K_o \mathbf{e} \tag{36}$$

$$A_i = -J^{-1}\left[\boldsymbol{\omega}\times\right]J \tag{37}$$

$$B_i = J^{-1} \tag{38}$$

$$A_i^T P_i + P_i A_i + Q_i - P_i B_i R_i^{-1} B_i^T P_i = O_3 \mapsto P_i > 0 \tag{39}$$

$$K_i = R_i^{-1} B_i^T P_i \tag{40}$$

$$L_i = -R_i^{-1} B_i^T (A_i - B_i K_i)^{-T} Q_i \tag{41}$$

$$\mathbf{u} = -K_i \boldsymbol{\omega} + L_i \boldsymbol{\omega}_c \tag{42}$$

Notice that the expression for $\mathbf{u}$ in Eq. (42) has been augmented with a term involving the command trajectory $\boldsymbol{\omega}_c$. Inserting Eq. (36) into Eq. (42) yields

$$\mathbf{u} = -\begin{bmatrix} K_i & L_i K_o \end{bmatrix}\begin{bmatrix} \boldsymbol{\omega} \\ \mathbf{e} \end{bmatrix} \tag{43}$$

which features the same structure as the SDRE single-loop controller from Eq. (28). Yet, since the overall closed-loop system is expected to follow $\boldsymbol{\omega}_c$ after some transient, the dual-loop controller performances are expected to be poorer than those of the single-loop controller. Also notice that the dual-loop SDRE controller involves the sequential solution of two 3×3 SDARE (34)(39), which represents significant computational savings with respect to solving the 6×6 SDARE of the single-loop controller.

3.3 Numerical simulation

Numerical simulations were run in order to compare the performances of the single-loop and dual-loop attitude controllers. The simulation equations consist of Eqs. (17),(18), where the control input $\mathbf{u}$ is computed using Eqs. (24)-(28) (single-loop) or Eqs. (33)-(42) (dual-loop). The S/C body-frame is assumed to have the following tensor of inertia J [kg-m^2] expressed in the body-frame $\mathcal{B}$:

$$J = \begin{bmatrix} 10 & -1 & -2 \\ -1 & 10 & -1 \\ -2 & -1 & 15 \end{bmatrix} \tag{44}$$

which is characteristic of a cubic-shape microsatellite. Each simulation runs over 100 seconds. The initial conditions and the values of the weight matrices are provided in Tables 1 and 2, respectively. Several measures of control performance are considered. CP1 [deg] is the Euclidean norm of the three mean angular errors in steady-state. The three means are time averages over the second-half of the simulation laps. The angular errors result from a 3-2-1 transformation from the quaternion $\mathbf{q}$ to Euler angles. CP2 [deg] is the norm of the three associated standard deviations. CP3 [rad/sec] and CP4 [rad/sec] are similar to CP1 and CP2 but are computed using the angular rates. CP1 to CP4 thus relate to the steady-state control performances. CP5 [N-m] is the maximum over time of the Euclidean norm of the control torque vector $\mathbf{u}$. CP6 [deg] and CP7 [rad/sec] are the maxima of the absolute values of the angular deviations and rates, respectively, over time and for all three axes. CP5, CP6, CP7 thus relate to the transient control performances. CP8 [N-m], CP9 [deg], and CP10 [rad/sec] are the l_2 norms of the sequences of control torques, 3-axes angular deviations, and 3-axes angular rates, respectively. The latter three "integral" measures of performances thus relate to both transient

and steady-state. Notice that the cost indexes of the optimal control problems were not used for the sake of comparison because the weight matrices are significantly different in the single-loop and dual-loop controllers. The performance measures CP8, CP9, and CP10 provide however a meaningful way to compare single-loop and dual-loop controllers and are themselves quadratic integral costs.
The comparison methodology is based on the following approach. First, weights for the single-loop controller (A in Table 1) are chosen in order to yield nominal performances in steady-state (both tracking error and settling time) and in control effort. Then the weights for the dual-loop controller are picked such as to guarantee similar steady-state performances as for controller A (B.a in Table 1). The key criteria is CP1, i.e. the angular tracking error. In addition, a different set of weights for the dual-loop controller was chosen in order to guarantee similar control effort as in controller A (B.b in Table 1). The key criteria are CP8 and CP9.
The results are summarized in Tables 3 and 4. Consider the results in CP1 for controllers A and B.a. Both controllers converge to zero and show similar settling times. Yet the controller B.a is slightly slower, inducing residual ripples in the angular tracking errors and thus higher value for the performance measure CP1. However, the essential difference resides in the control effort, as shown in the values for CP8. Controller A requires a torque of 0.87 [N-m] (l_2 norm) against 2.07 [N-m] for controller B.a.
The control weight R_i in controller B.b is 15 times higher than in controller B.a. This results in very close values for CP8 in controllers A and B.b, i.e. 0.87 [N-m] and 0.86 [N-m], respectively. Hence, the single-loop and dual-loop controllers require the same control energy. Comparing the values of CP1 and CP9 shows the performances gap. The angular tracking error CP1 in B.b is 108 [mdeg] against 0.1 [mdeg] in A. Further, the integral performance index CP9 is 83 [deg] in B.b against 73 [deg] in A. These drops in performances are direct consequences of a convergence slowdown in the system controlled by B.b, as a result of the increase of R_i. Notice that trials in correcting this gap by changing the outer-loop weights, i.e. by increasing Q_o in order to more penalize the angular tracking error, only created more ripples in the dynamics and in fact increased the integral cost CP9. Figures 1-f3 depict the time variations of the angular rates, the Euler angles, and the control torques. It is easy to see that the single-loop controller A compares advantageously with respect to either dual-loop controller B-a, which shows similar state transients but requires more control, or to dual-loop controller B-b, which applies similar control efforts but achieves slower and more oscilllatory transients.
As a concluding remark, both single-loop and dual-loop controllers can be designed to produce acceptable performances. The dual-loop controller exploits the cascaded structure of the S/C dynamics-kinematics equations. It features solutions of two 3×3 SDARE against a 6×6 SDARE for the single-loop controller. This represents substantial savings in the computational burden as full matrix products require $\mathcal{O}(n^3)$ operations (flops) and $\mathcal{O}(n^2)$ memory size for continuous or discrete ARE solving [12]. This beneficial effect should be traded against the loss in performances induced by the two-loop approach.

4. Attitude estimation without control

4.1 Preliminaries

Consider the angular velocity vector $\boldsymbol{\omega}$ and the quaternion $\mathbf{q}$, it is straightforward to prove the following identity:

$$\Xi(\mathbf{q})\,\boldsymbol{\omega} = \Omega(\boldsymbol{\omega})\,\mathbf{q} \tag{45}$$

where $\Xi(\mathbf{q})$ is defined in Eq. (19), i.e.:

$$\Xi(\mathbf{q}) = \begin{bmatrix} [\mathbf{e}\times] + q\,I_3 \\ -\mathbf{e}^T \end{bmatrix} \tag{46}$$

and $\Omega(\boldsymbol{\omega})$ is defined as follows:

$$\Omega(\boldsymbol{\omega}) = \begin{bmatrix} -[\boldsymbol{\omega}\times] & \boldsymbol{\omega} \\ -\boldsymbol{\omega}^T & 0 \end{bmatrix} \tag{47}$$

Let $\mathbf{b}$ and $\mathbf{r}$ denote the projections of a unit vector along the frames $\mathcal{B}$ and $\mathcal{R}$, respectively. They satisfy the following relation:

$$\mathbf{b} = A\,\mathbf{r} \tag{48}$$

where A denotes the rotation matrix from $\mathcal{R}$ to $\mathcal{B}$. Using Eq. (48) and the known relation between A and $\mathbf{q}$, the following relation can be developed:

$$\mathcal{H}\mathbf{q} = \mathbf{0} \tag{49}$$

where

$$\mathcal{H}(\mathbf{b}) = \begin{bmatrix} \frac{1}{2}\left[(\mathbf{b}+\ \mathbf{r})\times\right] & \frac{1}{2}\left(\mathbf{b}-\ \mathbf{r}\right) \\ -\frac{1}{2}\left(\mathbf{b}-\ \mathbf{r}\right)^T & 0 \end{bmatrix} \tag{50}$$

For any two vectors $\mathbf{b}_1, \mathbf{b}_2$, the following identity is easily shown:

$$\mathcal{H}(\mathbf{b}_1 + \mathbf{b}_2)\mathbf{q} = \mathcal{H}(\mathbf{b}_1)\mathbf{q} + \frac{1}{2}\,\Xi(\mathbf{q})\mathbf{b}_2 \tag{51}$$

where $\Xi(\mathbf{q})$ is defined in Eq. (46).

4.2 Model M2

In this case, the spacecraft is equipped with a triad of rate gyroscopes measuring $\boldsymbol{\omega}$ with a zero-mean additive white noise, $\boldsymbol{\epsilon}$, which intensity parameter σ_{ϵ} is of order 1 [deg/hour], which is typical for MEMS rate gyroscopes. Line-of-sight (LOS) measurements are acquired at a frequency of 10 [Hz] with additive zero-mean white noises. Their equivalent angular standard deviation σ_b is of order 1 [deg], which is typical for magnetometers. The SDRE filter, denoted F2, aims at estimating the quaternion. The model equations for the kinematics and the gyro measurement are as follows:

$$\dot{\mathbf{q}} = \frac{1}{2}\,\Omega(\boldsymbol{\omega}^{\rho})\mathbf{q} \tag{52}$$

$$\boldsymbol{\omega} = \boldsymbol{\omega}^{\rho} + \boldsymbol{\epsilon} \tag{53}$$

Using Eq. (53) in Eq. (52), and applying the identity (45), yields the design process equation:

$$\begin{aligned} \dot{\mathbf{q}} &= \frac{1}{2}\,\Omega(\boldsymbol{\omega} - \boldsymbol{\epsilon})\,\mathbf{q} \\ &= \frac{1}{2}\,\Omega(\boldsymbol{\omega})\,\mathbf{q} - \frac{1}{2}\,\Xi(\mathbf{q})\,\boldsymbol{\epsilon} \end{aligned} \tag{54}$$

The LOS measurement equation is as follows:

$$\mathbf{b}_k = A(\mathbf{q}_k)\mathbf{r}_k + \mathbf{v}_k \tag{55}$$

Using Eq. (55) in Eq. (49), and applying Eq. (51), yields the following design measurement equation:

$$\begin{aligned} \mathbf{0} &= \mathcal{H}(\,\mathbf{b}_k - \mathbf{v}_k)\,\mathbf{q}_k \\ &= \mathcal{H}(\,\mathbf{b}_k)\mathbf{q}_k - \frac{1}{2}\,\Xi(\mathbf{q}_k)\mathbf{v}_k \end{aligned} \tag{56}$$

The state-dependent coefficient (SDC) model M2 is summarized as follows:

$$\dot{\mathbf{q}} = \frac{1}{2}\,\Omega(\boldsymbol{\omega})\,\mathbf{q} - \frac{1}{2}\,\Xi(\mathbf{q})\,\boldsymbol{\epsilon} \tag{57}$$

$$\mathbf{z}_k = \mathcal{H}(\,\mathbf{b}_k)\mathbf{q}_k - \frac{1}{2}\,\Xi(\mathbf{q}_k)\mathbf{v}_k \tag{58}$$

where $\mathbf{z}_k$ is the zero vector. Tables 8 and 9 provides the characteristics of the model M2 required in order to implement the associated SDRE filter F2. The expression for the covariance matrix R of the measurement error stems from the unit-norm property of the LOS measurement $\mathbf{b}$. [cite]

4.3 Model M3

This case is identical to case 2 except for the angular rate measurement error, which includes gyro drifts in the three axes. The gyro drift vector, $\boldsymbol{\mu}_g$, is modeled as a Brownian motion. Hence:

$$\boldsymbol{\omega} = \boldsymbol{\omega}^{\rho} + \boldsymbol{\mu}_g + \boldsymbol{\epsilon} \tag{59}$$

$$\dot{\boldsymbol{\mu}}_g = \boldsymbol{\nu}_g \tag{60}$$

where $\boldsymbol{\nu}_g$ is a zero-mean white noise process with intensity parameter σ_{ng}. The values for the initial drift, $\boldsymbol{\mu}_g(0)$, and σ_{ng} appear in Table 1 and 5, respectively. Combining Eqs. (52), (59), and (60) yields

$$\begin{bmatrix}\dot{\mathbf{q}}\\ \dot{\boldsymbol{\mu}}_g\end{bmatrix} = \begin{bmatrix}\frac{1}{2}\,\Omega(\boldsymbol{\omega}-\boldsymbol{\mu}_g-\boldsymbol{\epsilon})\,\mathbf{q}\\ \boldsymbol{\nu}_g\end{bmatrix} \tag{61}$$

$$= \begin{bmatrix}\frac{1}{2}\,\Omega(\boldsymbol{\omega}-\boldsymbol{\mu}_g)\,\mathbf{q}\\ \mathbf{0}\end{bmatrix} + \begin{bmatrix}-\frac{1}{2}\,\Xi(\mathbf{q})\,\boldsymbol{\epsilon}\\ \boldsymbol{\nu}_g\end{bmatrix} \tag{62}$$

$$= \begin{bmatrix}\frac{1}{2}\,\Omega(\boldsymbol{\omega}) & -\frac{1}{2}\,\Xi(\mathbf{q})\\ O_{34} & O_3\end{bmatrix}\begin{bmatrix}\mathbf{q}\\ \boldsymbol{\mu}_g\end{bmatrix} + \begin{bmatrix}-\frac{1}{2}\,\Xi(\mathbf{q}) & O_{43}\\ O_{34} & I_3\end{bmatrix}\begin{bmatrix}\boldsymbol{\epsilon}\\ \boldsymbol{\nu}_g\end{bmatrix} \tag{63}$$

Equation (45) was used successively in order to derive Eq. (62) and Eq. (63). The first term in the right-hand-side (RHS) of Eq. (62) provides the deterministic part of the nonlinear model and its SDC expression appears in Eq. (63). The measurement model equation is identical to that of model M2 except for the expression of the SDC measurement matrix. The SDC measurement equation for M3 is thus as follows:

$$\mathbf{z}_k = \begin{bmatrix}\mathcal{H}(\,\mathbf{b}_k) & O_{43}\end{bmatrix}\begin{bmatrix}\mathbf{q}_k\\ \boldsymbol{\mu}_g(k)\end{bmatrix} - \frac{1}{2}\,\Xi(\mathbf{q}_k)\mathbf{v}_k \tag{64}$$

In order to illustrate the non-uniqueness of the SDC models, consider the following matrix, $\begin{bmatrix}\frac{1}{2}\,\Omega(\boldsymbol{\omega}-\boldsymbol{\mu}_g) & O_{43}\\ O_{34} & O_3\end{bmatrix}$, which is a valid SDC dynamics matrix that can be used in Eq. (63). Yet, it is obvious that such a choice would yields a pointwise unobservable system, where the drift can not be estimated.

4.4 Model M4

The model M4 includes all assumptions of M3 and in addition assumes that the LOS measurement is corrupted by a three-axes bias, $\boldsymbol{\mu}_b$. This process is modeled as a Brownian motion driven by a zero-mean white noise, $\boldsymbol{\nu}_b$, with intensity parameter σ_{nb}. Hence,

$$\dot{\boldsymbol{\mu}}_b = \boldsymbol{\nu}_b \tag{65}$$

The values of $\boldsymbol{\mu}_b(0)$ and σ_{nb} are provided in Tables 1 and 5, respectively. Appending Eq. (65) to Eq. (61), and using similar steps than for Eqs. (62)-(63) yields

$$\begin{bmatrix}\dot{\mathbf{q}}\\ \dot{\boldsymbol{\mu}}_g\\ \dot{\boldsymbol{\mu}}_b\end{bmatrix} = \begin{bmatrix}\frac{1}{2}\,\Omega(\boldsymbol{\omega}-\boldsymbol{\mu}_g)\,\mathbf{q}\\ \mathbf{0}\\ \mathbf{0}\end{bmatrix} + \begin{bmatrix}-\frac{1}{2}\,\Xi(\mathbf{q})\,\boldsymbol{\epsilon}\\ \boldsymbol{\nu}_g\\ \boldsymbol{\nu}_b\end{bmatrix} \tag{66}$$

$$= \begin{bmatrix}\frac{1}{2}\,\Omega(\boldsymbol{\omega}) & -\frac{1}{2}\,\Xi(\mathbf{q}) & O_{43}\\ O_{34} & O_3 & O_3\\ O_{34} & O_3 & O_3\end{bmatrix}\begin{bmatrix}\mathbf{q}\\ \boldsymbol{\mu}_g\\ \boldsymbol{\mu}_b\end{bmatrix} + \begin{bmatrix}-\frac{1}{2}\,\Xi(\mathbf{q}) & O_{43} & O_{43}\\ O_{34} & I_3 & O_3\\ O_3 & O_3 & I_3\end{bmatrix}\begin{bmatrix}\boldsymbol{\epsilon}\\ \boldsymbol{\nu}_g\\ \boldsymbol{\nu}_b\end{bmatrix} \tag{67}$$

The LOS measurement is modeled as follows:

$$\mathbf{b}_k = A(\mathbf{q}_k)\mathbf{r}_k + \boldsymbol{\mu}_b(k) + \mathbf{v}_k \tag{68}$$

Using Eq. (68) in Eq. (49) and using Eq. (51) twice yields the following equations:

$$\mathbf{z}_k = \mathcal{H}(\,\mathbf{b}_k - \boldsymbol{\mu}_b(k) - \mathbf{v}_k)\,\mathbf{q}_k$$

$$= \mathcal{H}(\,\mathbf{b}_k - \boldsymbol{\mu}_b(k))\mathbf{q}_k - \frac{1}{2}\,\Xi(\mathbf{q}_k)\mathbf{v}_k \tag{69}$$

$$= \begin{bmatrix}\mathcal{H}(\,\mathbf{b}_k) & O_{43} & -\frac{1}{2}\,\Xi(\mathbf{q}_k)\end{bmatrix}\begin{bmatrix}\mathbf{q}_k\\ \boldsymbol{\mu}_g(k)\\ \boldsymbol{\mu}_b(k)\end{bmatrix} - \frac{1}{2}\,\Xi(\mathbf{q}_k)\mathbf{v}_k \tag{70}$$

where $\mathbf{z}_k = \mathbf{0}$. The deterministic parts of the nonlinear process and measurement equations appear in the first terms of the RHS of Eqs. (66) and (69), respectively. Equations (67) and (70) feature the SDC model for M4 on which the SDRE filter F4 is applied.

4.5 Model M5

In this case, the LOS measurements are corrupted with white noises only, like in the model M2, and there are no available measurements of the angular rates. The process equations consist thus of Eqs. (17),(18), with no control, i.e.

$$\begin{bmatrix}\dot{\boldsymbol{\omega}}\\ \dot{\mathbf{q}}\end{bmatrix} = \begin{bmatrix}-J^{-1}\,[\boldsymbol{\omega}\times]\,J\boldsymbol{\omega}\\ \frac{1}{2}\,\Omega(\boldsymbol{\omega})\,\mathbf{q}\end{bmatrix} + \begin{bmatrix}\mathbf{n}_\omega\\ O_{43}\end{bmatrix} \tag{71}$$

$$= \begin{bmatrix}-J^{-1}\,[\boldsymbol{\omega}\times]\,J & O_{34}\\ \frac{1}{2}\,\Xi(\mathbf{q}) & O_4\end{bmatrix}\begin{bmatrix}\boldsymbol{\omega}\\ \mathbf{q}\end{bmatrix} + \begin{bmatrix}I_3\\ O_{43}\end{bmatrix}\mathbf{n}_\omega \tag{72}$$

where $\mathbf{n}_\omega$ represents modeling errors in the rigid-body dynamics. This process is modeled as a zero-mean white noise with intensity parameter σ_ω, which was chosen via trial and errors as 10^{-9} [rad/sec$^{3/2}$]. Extensive simulations of the filter F5 showed that no process noise needed to be added to the design process equation of the quaternion. Equation (71) features the deterministic part of the nonlinear process model and Eq. (72) shows the proposed SDC model M5. The measurement is identical to M2 with a modified SDC measurement matrix, as follows:

$$\mathbf{z}_k = \begin{bmatrix}O_{43} & \mathcal{H}(\,\mathbf{b}_k)\end{bmatrix}\begin{bmatrix}\boldsymbol{\omega}_k\\ \mathbf{q}_k\end{bmatrix} - \frac{1}{2}\,\Xi(\mathbf{q}_k)\mathbf{v}_k \tag{73}$$

In order to illustrate the non-uniqueness of SDC modeling, it is noticed that the dynamics matrix $\begin{bmatrix}-J^{-1}\,[\boldsymbol{\omega}\times]\,J & O_{34}\\ O_{43} & \frac{1}{2}\,\Omega(\boldsymbol{\omega})\end{bmatrix}$ is a valid SDC matrix in Eq. (72), but provides, together with the measurement model, a pointwise unobservable system for the angular rate vector.

4.6 Model M6

The LOS measurements incorporate a bias, like in M4, and there are no rate gyroscopes, like in M5. The model M6 is thus a combination of the kinematics and dynamics as modeled in M5, and of the measurement equation of M4. Henceforth, the process equations are written as follows:

$$\begin{bmatrix}\dot{\boldsymbol{\omega}}\\ \dot{\mathbf{q}}\\ \dot{\boldsymbol{\mu}}_b\end{bmatrix} = \begin{bmatrix}-J^{-1}\,[\boldsymbol{\omega}\times]\,J\boldsymbol{\omega}\\ \frac{1}{2}\,\Omega(\boldsymbol{\omega})\,\mathbf{q}\\ \mathbf{0}\end{bmatrix} + \begin{bmatrix}\mathbf{n}_\omega\\ \mathbf{0}\\ \boldsymbol{\nu}_b\end{bmatrix} \tag{74}$$

$$= \begin{bmatrix}-J^{-1}\,[\boldsymbol{\omega}\times]\,J & O_{34} & O_3\\ \frac{1}{2}\,\Xi(\mathbf{q}) & O_4 & O_{43}\\ O_3 & O_{34} & O_3\end{bmatrix}\begin{bmatrix}\boldsymbol{\omega}\\ \mathbf{q}\\ \boldsymbol{\nu}_b\end{bmatrix} + \begin{bmatrix}I_3 & O_3\\ O_{43} & O_{43}\\ O_3 & I_3\end{bmatrix}\begin{bmatrix}\mathbf{n}_\omega\\ \mathbf{n}_b\end{bmatrix} \tag{75}$$

The SDC matrices are identified from Equation (75). The SDC measurement matrix is identified from the following measurement equation:

$$\mathbf{z}_k = \mathcal{H}(\,\mathbf{b}_k - \boldsymbol{\mu}_b(k))\mathbf{q}_k - \frac{1}{2}\,\Xi(\mathbf{q}_k)\mathbf{v}_k \tag{76}$$

$$= \begin{bmatrix}O_{43} & \mathcal{H}(\,\mathbf{b}_k) & -\frac{1}{2}\,\Xi(\mathbf{q}_k)\end{bmatrix}\begin{bmatrix}\boldsymbol{\omega}_k\\ \mathbf{q}_k\\ \boldsymbol{\mu}_b(k)\end{bmatrix} - \frac{1}{2}\,\Xi(\mathbf{q}_k)\mathbf{v}_k \tag{77}$$

where $\mathbf{z}_k$ is the null vector.

4.7 Filters implementation

The previous subsections presented the developments of five various state-space models, M2-M6, where the deterministic parts and the SDC matrices could be identified. Theses quantities correspond to the functions and matrices $f(\mathbf{x})$, $h(\mathbf{x})$, $F(\mathbf{x})$, $G(\mathbf{x})$, $H(\mathbf{x})$, $\Gamma(\mathbf{x})$, that are required in order to implement the associated SDRE filters F2-F6. All these quantities are summarized in Tables 8 and 9 for each model.

Measurement update stage Since the measurement vector in Eq. (15) is identically zero, the measurement update stage equation is simplified to:

$$\widehat{\mathbf{x}}_{k+1/k+1} = \left[I - K_{k+1}H(\widehat{\mathbf{x}}_{k+1/k})\right]\widehat{\mathbf{x}}_{k+1/k} \tag{78}$$

Notice that for the sake of maintaining the norm of the estimated quaternion unity, the estimated quaternion is normalized after each measurement update by dividing it with its Euclidean norm. No tuning was needed in filters F2 and F3. In filters F4, F5, and F6, the filter value of σ_b was increased by a factor 10. In filters F5 and F6, the intensity parameter $\sigma_\omega = 10^{-9}$ [rad/sec$^{3/2}$]. The covariance matrices $\Gamma R \Gamma^T$ are rank deficient. Yet, due to the constantly changing values of the LOS measurements, and thus of the measurement matrices, the covariance matrices S_{k+1} are not singular, and the filters covariance computations are numerically well-behaved.

4.8 Numerical simulation

The spacecraft is assumed to rotate around its center of mass without external torque. The initial conditions for the states, the estimation errors, and the associated covariance matrices are provided in Tables 1, 6, and 7. The values of the sensors intensity parameters appear in Table 5. In order to compare the performances of the various filters, eight Estimation Performance criteria, EP1-8, were computed. The measures EP1 [deg] and EP2 [deg] are the time average and standard deviation of the angular estimation error in steady-state, i.e. over the last 50 seconds (half of the simulation laps). The measures EP3 [rad/sec] and EP4 [rad/sec] consist of similar indexes calculated from the history of the Euclidean norm of the angular velocity estimation error vector. The latter is computed using as the difference between the true and the estimated rate vector. The estimated rate vector is simply the measured rate vector in F2, it is the measured rate corrected with the estimated gyro biases in F3-F4, and it is a filter output in F5-F6. The measures EP5-6 [rad/sec] and EP7-8 [rad] are computed similarly to EP3-4 using the Euclidean norms of the gyro drift and line-of-sight bias estimation error vectors, respectively. Table 10 summarizes the results for the SDRE filters F2 to F6. The table shows that the filters using gyro measurements, F2-4 provide similar EP1 results for the average angular error, appr. 70 [mdeg]. Comparing this value to the LOS measurement angular error of 500 [mdeg] ($\sigma_b = 10^{-2}$ [rad]) shows the effectiveness of the filtering. It appears clearly that the dispersion EP2 is higher when the filters incorporate additional states like gyro drifts and LOS biases. In addition, the filters estimating the angular velocity, F5,F6, reach a slightly degraded angular error performance level, about 80-90 [mdeg], and similar standard deviations as the gyro-based filters. The averages EP3 in the angular rates are also higher in the gyroless filters (110-125 [microrad/sec]) than in the gyro-based ones (50-70 [microrad/sec]). On the other hand, the dispersions EP4 in the angular rates error are significantly lower in the gyroless filters (115-126 [microrad/sec] versus 545-551 [microrad/sec]) thanks to the filtering effect and the absence of gyro measurement white noise in the estimation errors. It is not surprising that the performance indexes EP5 and EP6 are slightly degraded between filters F3 and F4, due to additional states in the estimator F4. Interestingly, the measures EP7 and EP8 are very similar in the gyro-based filter F4 and the gyroless filter F6, yielding averages of 7 and 6 [mrad] and standard deviations of 790 and 776 [microrad], respectively.
Further comparison between the gyro-based and gyroless filters are obtained by plotting the time-histories of the estimation errors in the angular rates, the angular error, the quaternion components, the angular rates, the gyro drifts, and the LOS biases. The plots of these errors appear in Figs. 4-8, respectively, for filters F2, F4, and F6. Filters F4 and F6 are the most elaborated in the current study and allow for comparison of the gyro-based and gyroless approach under realistic noise modeling. Filter F2 is provided for comparison, as it is based on the simplest and thus most ideal case for the attitude error. Figure 4 shows that the gyroless filter F6 features less noisy performances than the gyro-based filters F2, F4. The error in F2 is merely the gyro measurement white noise. It appears that the error in F6 converges to the same level of error. Both gyro-based filters have shorter transients (10 [sec]) than the gyroless filter F6 (20 [sec]). Figure 5 shows that filters F4 and F6 perform similarly with respect to the angular estimation point of view. From Fig. 6 it is seen that the errors in the quaternion in F4 are noisier than in filter F6, as a result of the gyro drift estimation. The performance in the estimation of the drift in F4 are depicted in Fig. 7 for each component. The single run plots reveal unbiasedness and steady-state levels around 10^{-4} [rad/sec], which are acceptable for the given gyro drifts (similar values after 100 seconds). Figure 8 shows that the estimation errors in the LOS biases are biased around 2-5 [mrad] for each component and that the errors are slightly smoother in F6. The LOS biases, which values are 10 [mrad], were thus partially estimated.

5. Combined SDRE estimation and control

This section presents numerical results on the performances of the single-loop and dual-loop controllers, A and B.a, developed in sections 3, but with partial information. The feedback loop implements a linear feedback of the estimated rate and quaternion that are provided by the filters developed in section 4. For the sake of brevity, the following three filters are implemented: filter F2, where only the quaternion is estimated, filter F4, where the quaternion, the gyro drifts, and the LOS biases are estimated, and filter F6, where the quaternion, the angular rates, and the LOS biases are estimated. The combined SDRE filter-based controllers are denoted using the single/dual loop symbol and the filter symbol, e.g. AF2.

Tables 11 and 12 summarize the findings about the impact of the estimation on the control performances. Table 11 shows the control performances measures, CP1-CP7, for the cases A, AF2, AF4, and AF6. When implementing the gyro-based filters (AF2-4) the performances degrade in CP1 and in CP3, the steady-state performances in angle and rate, but they are similar in CP5-7, i.e. transients. On the other hand, estimating the angular velocity (AF6) instead of measuring/correcting it (AF2/Af4) brings better steady-state performances for the rates averages and deviations (CP3-4) and for the angular deviations (CP2). The steady-state of the controller signals seems smoother using a rate estimator. On the other hand, the transients are lower when using the gyro in the controller, as seen from CP5-7 between AF4 and AF6. Table 12 summarizes the results for the dual-loop controller with partial information. Here again, as seen from CP3-4 between the controller BaF4 and BaF6, using a rate estimator provides smoother transients than using a gyro. In particular, the performances degrade dramatically from BaF2 to BaF4. This shows how the estimation of the LOS bias is critical to the overall control performances. As seen from CP1, there is a consistent degradation in angle performances from A to AF6. Further, the maxima, CP5-7, seem insensitive to the filter choice, when using the gyro, but they increase when using a rate estimator. Figure 9 depicts the variations of the controlled rates with controllers A, AF2, AF4, and AF6. The plots show that the controller AF2 performs similarly to the full information case, A. The noisiest controller is AF4 and the slowest is AF6. On the other hand, it appears clearly that AF6 is smoother than AF4. Figure 10 zooms on the steady-state of the angles for the various controllers. It appears that AF2 follows well the ideal trajectory of A, and that the other controllers show some biases in their performances, of order 0.2 [deg]. Figure 11 shows the time variations of the control torques, and clearly depict the noisiness of the gyro-based controllers, with deviations of order 0.005 N-m, and the relative smoothness (and delay) of the rate-estimator based controller.

Further simulations were run in order to investigate the impact of the controllers on the estimation performances. Figure 12 summarizes the results. Figure 12-a presents the angular estimation error as a function of time for the control-free estimator F2, and the controlled cases, AF2 and BaF2. Clearly, the control-free case has better transient and steady-state levels than the controlled cases. This is an illustration of the conflicting tasks of estimation and control, where some *persistency* of the signals is required in order to provide enough observability. Notice that the two controllers have similar performances in steady-state. Figure 12-b, on the other hand, shows that all three cases with filter F4 have similar performances. Figure 12-c depict the angular estimation errors for the three cases with the filter F6. The control-free case has got better performances in steady-state, and both controllers have similar transients and identical steady-state levels.

6. Conclusion

This work presented the development of several State-Dependent Riccati Equation filters and controllers for attitude determination and control of a rigid-body spacecraft. The development was systematic by designing single-loop and dual-loop controllers, where filters estimated the attitude quaternion, the attitude rates, and sensors biases. With the given mid-grade gyros and the line-of-sight accuracy of 0.5 deg, the angular estimation error average is around 0.1 deg. It appears that the gyroless estimation performances are smoother and more accurate in steady-state, but the gyro-based estimation performances have better convergence properties. Estimation performances turn to be enhanced in the control-free case, whether or not gyros are used. This effectively illustrates the antagonistic natures of estimation and control. Both single-loop and dual-loop controllers provide satisfactory results with estimators in the loop. Overall, the pointing control performance is almost entirely dictated by the estimators performance. The dual-loop approach requires less computations but suffers a loss in pointing performance relative to the single-loop. For similar pointing performances, in the averages and standard deviations of the angles and rates, the required control is twice as large, for the maxima and the integral criteria. For similar values of the control energy, the dual-loop responses in angles and rates are significantly slower than with the single-loop. However, the maximum control value is slightly lower; this is characteristics to multiple-loops controllers which tend to show smoother responses than the corresponding single-loop controller. Future works will address the actuation modeling, in particular the potential saturation, the external torques modeling, additional investigation on the performances loss due to the cascaded approach and on the dual effect of control and estimation.

Acknowledgements

The first author was supported by THE ISRAEL SCIENCE FOUNDATION (grant No. 1546/08).

References

[1] Wertz, J.R. (ed.), *Spacecraft Attitude Determination and Control*, D. Reidel, Dordrecht, The Netherlands, 1984.

[2] Cloutier, J.R., "State-Dependent Riccati Equation Techniques: an Overview," *Proceedings of the American Control Conference* , Albuquerque, New Mexico, June, 1997, pp. 932–936.

[3] Cimen, T., "State-Dependent Riccati Equation (SDRE) Control: A Survey," *Proceedings of the 17th World Congress, The International Federation of Automatic Control*, Seoul, Korea, July 6-11, 2008, pp. 3761–3775.

[4] Parrish, D.K., and Ridgely, D.B., "Attitude Control of a Satellite using the SDRE Method," *Proceedings of the American Control Conference* , Albuquerque, New Mexico, June, 1997, pp. 942–946.

[5] Stansbery, D.T., Cloutier, J.R., "Position and Attitude Control of a Spacecraft using the State-Dependent Riccati Equation Technique," *Proceedings of the American Control Conference* , Chicago, Illinois, June, 2000, pp. 1867–1871.

[6] Bar-Itzhack, I.Y., Harman, R.R., "Pseudolinear and State-Dependent Riccati Equation Filtersfor Angular Rate Estimation," *Journal of Guidance, Control, and Dynamics*, Vol. 22, No. 5, 1999, pp. 723–725.

[7] Bar-Itzhack, I.Y., Harman, R.R., Choukroun, D., "State-Dependent Pseudo-Linear Filters for Spacecraft Attitude and Rate Estimation," *Proceedings of the AIAA Guidance, Navigation, and Control Conference*, AIAA 2002-4461, Monterey, CA, Aug. 2002.

[8] Abdelrahman, M., Park, S.Y., "Integrated Attitude Determination and Control System via Magnetic Measurements and Actuation," *Acta Astronautica*, (69), 2011, pp. 168–185.

[9] Haim, L., Choukroun, D., "Optimizaed State-Dependent Riccati Equation Method for Spacecraft Attitude Estimation and Control," *Proceedings of the AIAA Guidance, Navigation, and Control Conference*, AIAA 2012-4557, Minneapolis, MN, Aug. 2012.

[10] Masssari, M., Zamaro, M., "Application of SDRE Technique to Orbital and Attitude Control of Spacecraft Formation Flying," *Acta Astronautica*, (2013), http://dx.doi.org/10.1016/j.actaastro.2013.02.001

[11] Choukroun, D., Oshman, Y., and Bar-Itzhack, I.Y., "Novel Quaternion Kalman Filter," *IEEE Transactions on Aerospace and Electronic Systems*, Vol. AC-42, No. 1, Jan. 2006, pp. 174–190.

[12] Datta, B., *Numerical Methods for Linear Control Systems*, Elsevier Academic Press, Boston, 2004.

[13] Tekinalp, O., Unlu, T., Yavrucuk, I., "Simulation and Flight Control of a Tilt-Duct UAV," *AIAA Modeling and Simulation Technologies Conference*, Chicago, IL, 10-13 Aug. 2009.

[14] Kayastha, S., Tekinalp, O., Ozgoren, K., "Quaternion Based State Dependent Ricatti Equation Control of a Satellite Camera on Piezoelectric Actuators," *AIAA Astrodynamics Specialist Conference*, Toronto, Canada, 2-5 Aug. 2010.

Table 1: Initial values for the angular rates, the Euler angles, the gyro drift and the line-of-sight bias

$\boldsymbol{\omega}(0)$ [rad/sec]	$(\phi, \theta, \psi)(0)$ [deg]	$\boldsymbol{\mu}_g(0)$ [rad/sec]	$\boldsymbol{\mu}_b(0)$ [rad]
$(10^{-2}, 10^{-2}, 10^{-2})$	$(25, 25, 25)$	$(10^{-5}, 10^{-5}, 10^{-5})$	$(10^{-2}, 10^{-2}, 10^{-2})$

Table 2: Values of the weight matrices in the cost functions for single-loop and dual-loop controllers

Controller	Loop	State Weight	Control Weight
A	Single-loop	$Q = \text{diag}(\, I_{_3}, 50\, I_{_3})$	$R = 10\, I_{_3}$
B.a	Dual-loop	$Q_i = 30\, I_{_3}, Q_o = \, I_{_3}$	$R_i = \, I_{_3}, R_o = \, I_{_3}$
B.b	Dual-loop	$Q_i = 30\, I_{_3}, Q_o = \, I_{_3}$	$R_i = 15\, I_{_3}, R_o = \, I_{_3}$

Table 3: Control performances of single-loop and dual-loop controllers. CP1-CP7: Steady-state and Transient

Controller	$10^3\times$CP1 [deg]	$10^3\times$CP2 [deg]	$10^6\times$CP3 [rad/sec]	$10^6\times$CP4 [rad/sec]	$10^2\times$CP5 [N-m]	CP6 [deg]	$10^3\times$CP7 [rad/sec]
A	0.10	0.29	0.43	0.91	46	27	68
B.a	0.12	0.70	1.12	3.96	106	27	120
B.b	108.00	554.00	445.00	2624.00	30	27	82

Table 4: Control performances of single-loop and dual-loop controllers. CP8-CP10: Integral

Controller	$10^2\times$CP8 [N-m]	CP9 [deg]	$10^2\times$CP10 [rad/sec]
A	87	73	24
B.a	207	60	34
B.b	86	83	33

Table 5: Intensity parameters of the white noises in the gyros and the line-of-sight (LOS) measurement errors

Gyro Noise $\sigma_v\ [\frac{rad}{\sqrt{sec}}]$	Gyro Drift $\sigma_{ng}\ [\frac{rad}{sec^{3/2}}]$	LOS Noise $\sigma_b\ [rad]$	LOS Bias $\sigma_{nb}\ [\frac{rad}{\sqrt{sec}}]$
10^{-4}	10^{-5}	10^{-2}	10^{-4}

Table 6: Initial estimation errors in the rates, the Euler angles, the gyro drift and the line-of-sight bias

$\widetilde{\boldsymbol{\omega}}(0)$ [rad/sec]	$\widetilde{(\phi,\theta,\psi)}(0)$ [deg]	$\widetilde{\boldsymbol{\mu}}_g(0)$ [rad/sec]	$\widetilde{\boldsymbol{\mu}}_b(0)$ [rad]
$(0.2, 0.2, 0.2)$	$(25, 25, 25)$	$(10^{-4}, 10^{-4}, 10^{-4})$	$(0.5, 0.5, 0.5)$

Table 7: Initial values of the estimation error covariance matrices for the various filters

	F2	F3	F4	F5	F6
$\boldsymbol{\omega}$				$0.5\, I_3$	$0.5\, I_3$
$\mathbf{q}$	$10^{-1}\, I_4$	$10^{-1}\, I_4$	$10^{-1}\, I_4$	$10^{-4}\, I_4$	$10^{-4}\, I_4$
$\boldsymbol{\mu}_g$		$10^{-4}\, I_3$	$10^{-4}\, I_3$		
$\boldsymbol{\mu}_b$			I_3		I_3

Table 8: Process - Nonlinear state-space models and their related state-dependent coefficients. Ω is defined in Eq. (47). Ξ is defined in Eq. (46).

	$\mathbf{x}$	$f(\mathbf{x})$	$F(\mathbf{x})$	$G(\mathbf{x})$	W
M2	$\mathbf{q}$	$\frac{1}{2}\,\Omega(\boldsymbol{\omega})\,\mathbf{q}$	$\frac{1}{2}\,\Omega(\boldsymbol{\omega})$	$-\frac{1}{2}\,\Xi(\mathbf{q})$	$\sigma_{\epsilon}^2\, I_3$
M3	$\begin{bmatrix}\mathbf{q}\\ \boldsymbol{\mu}_g\end{bmatrix}$	$\begin{bmatrix}\frac{1}{2}\,\Omega(\boldsymbol{\omega}-\boldsymbol{\mu}_g)\,\mathbf{q}\\ \mathbf{0}\end{bmatrix}$	$\begin{bmatrix}\frac{1}{2}\,\Omega(\boldsymbol{\omega}) & -\frac{1}{2}\,\Xi(\mathbf{q})\\ O_{34} & O_3\end{bmatrix}$	$\begin{bmatrix}-\frac{1}{2}\,\Xi(\mathbf{q}) & O_{43}\\ O_{34} & I_3\end{bmatrix}$	$\begin{bmatrix}\sigma_{\epsilon}^2\, I_3 & O_3\\ O_3 & \sigma_{ng}^2\, I_3\end{bmatrix}$
M4	$\begin{bmatrix}\mathbf{q}\\ \boldsymbol{\mu}_g\\ \boldsymbol{\mu}_b\end{bmatrix}$	$\begin{bmatrix}\frac{1}{2}\,\Omega(\boldsymbol{\omega}-\boldsymbol{\mu}_g)\,\mathbf{q}\\ \mathbf{0}\\ \mathbf{0}\end{bmatrix}$	$\begin{bmatrix}\frac{1}{2}\,\Omega(\boldsymbol{\omega}) & -\frac{1}{2}\,\Xi(\mathbf{q}) & O_{43}\\ O_{34} & O_3 & O_3\\ O_{34} & O_3 & O_3\end{bmatrix}$	$\begin{bmatrix}-\frac{1}{2}\,\Xi(\mathbf{q}) & O_{43} & O_{43}\\ O_3 & I_3 & O_3\\ O_3 & O_3 & I_3\end{bmatrix}$	$\begin{bmatrix}\sigma_{\epsilon}^2\, I_3 & O_3 & O_3\\ O_3 & \sigma_{ng}^2\, I_3 & O_3\\ O_3 & O_3 & \sigma_{nb}^2\, I_3\end{bmatrix}$
M5	$\begin{bmatrix}\boldsymbol{\omega}\\ \mathbf{q}\end{bmatrix}$	$\begin{bmatrix}-J^{-1}\,[\boldsymbol{\omega}\times]\,J\boldsymbol{\omega}\\ \frac{1}{2}\,\Omega(\boldsymbol{\omega})\,\mathbf{q}\end{bmatrix}$	$\begin{bmatrix}-J^{-1}\,[\boldsymbol{\omega}\times]\,J & O_{34}\\ \frac{1}{2}\,\Xi(\mathbf{q}) & O_4\end{bmatrix}$	$\begin{bmatrix}I_3\\ O_{43}\end{bmatrix}$	$\sigma_{\omega}^2\, I_3$
M6	$\begin{bmatrix}\boldsymbol{\omega}\\ \mathbf{q}\\ \boldsymbol{\mu}_b\end{bmatrix}$	$\begin{bmatrix}-J^{-1}\,[\boldsymbol{\omega}\times]\,J\boldsymbol{\omega}\\ \frac{1}{2}\,\Omega(\boldsymbol{\omega})\,\mathbf{q}\\ \mathbf{0}\end{bmatrix}$	$\begin{bmatrix}-J^{-1}\,[\boldsymbol{\omega}\times]\,J & O_{34} & O_3\\ \frac{1}{2}\,\Xi(\mathbf{q}) & O_4 & O_{43}\\ O_3 & O_{34} & O_3\end{bmatrix}$	$\begin{bmatrix}I_3 & O_3\\ O_{43} & O_{43}\\ O_3 & I_3\end{bmatrix}$	$\begin{bmatrix}\sigma_{\omega}^2\, I_3 & O_3\\ O_3 & \sigma_{nb}^2\, I_3\end{bmatrix}$

Table 9: Measurement - Nonlinear state-space models and their related state-dependent coefficients. $\mathcal{H}$ is defined in Eq. (50). Ξ is defined in Eq. (46).

	$\mathbf{x}$	$h(\mathbf{x})$	$H(\mathbf{x})$	$\Gamma(\mathbf{x})$	R
M2	$\mathbf{q}$	$\mathcal{H}(\mathbf{b})\,\mathbf{q}$	$\mathcal{H}(\mathbf{b})$	$-\frac{1}{2}\,\Xi(\mathbf{q})$	$\sigma_b^2(\,I_3-\mathbf{b}\mathbf{b}^T)$
M3	$\begin{bmatrix}\mathbf{q} & \boldsymbol{\mu}_g\end{bmatrix}$	$\mathcal{H}(\mathbf{b})\,\mathbf{q}$	$\begin{bmatrix}\mathcal{H}(\mathbf{b}) & O_{43}\end{bmatrix}$	$-\frac{1}{2}\,\Xi(\mathbf{q})$	$\sigma_b^2(\,I_3-\mathbf{b}\mathbf{b}^T)$
M4	$\begin{bmatrix}\mathbf{q} & \boldsymbol{\mu}_g & \boldsymbol{\mu}_b\end{bmatrix}$	$\mathcal{H}(\mathbf{b}-\boldsymbol{\mu}_b)\,\mathbf{q}$	$\begin{bmatrix}\mathcal{H}(\mathbf{b}) & O_{43} & -\frac{1}{2}\,\Xi(\mathbf{q})\end{bmatrix}$	$-\frac{1}{2}\,\Xi(\mathbf{q})$	$\sigma_b^2(\,I_3-\mathbf{b}\mathbf{b}^T)$
M5	$\begin{bmatrix}\boldsymbol{\omega} & \mathbf{q}\end{bmatrix}$	$\mathcal{H}(\mathbf{b})\,\mathbf{q}$	$\begin{bmatrix}O_{43} & \mathcal{H}(\mathbf{b})\end{bmatrix}$	$-\frac{1}{2}\,\Xi(\mathbf{q})$	$\sigma_b^2(\,I_3-\mathbf{b}\mathbf{b}^T)$
M6	$\begin{bmatrix}\boldsymbol{\omega} & \mathbf{q} & \boldsymbol{\mu}_b\end{bmatrix}$	$\mathcal{H}(\mathbf{b}-\boldsymbol{\mu}_b)\,\mathbf{q}$	$\begin{bmatrix}O_{43} & \mathcal{H}(\mathbf{b}) & -\frac{1}{2}\,\Xi(\mathbf{q})\end{bmatrix}$	$-\frac{1}{2}\,\Xi(\mathbf{q})$	$\sigma_b^2(\,I_3-\mathbf{b}\mathbf{b}^T)$

Table 10: Estimation performances of the SDRE filters. Control-free case.

Filter	$10^3\times$EP1 [deg]	$10^3\times$EP2 [deg]	$10^6\times$EP3 [rad/sec]	$10^6\times$EP4 [rad/sec]	$10^6\times$EP5 [rad/sec]	$10^6\times$EP6 [rad/sec]	$10^3\times$EP7 [rad]	$10^6\times$EP8 [rad]
F2	73	15	50	545	n/a	n/a	n/a	n/a
F3	74	46	70	551	53	54	n/a	n/a
F4	73	47	72	551	78	63	7	790
F5	83	40	110	115	n/a	n/a	n/a	n/a
F6	94	40	125	126	n/a	n/a	6	776

Table 11: Control performances of the single-loop controller A with various filters. Steady-state and Transient

Controller	$10^3\times$CP1 [deg]	$10^3\times$CP2 [deg]	$10^6\times$CP3 [rad/sec]	$10^6\times$CP4 [rad/sec]	$10^2\times$CP5 [N-m]	CP6 [deg]	$10^3\times$CP7 [rad/sec]
A	0.10	0.29	0.43	0.91	46	27	68
AF2	139	30	11	108	70	27	68
AF4	164	126	96	543	70	27	58
AF6	175	71	37	287	156	45	161

Table 12: Control performances of the dual-loop controller B.a with various filters. Steady-state and Transient

Controller	$10^3\times$CP1 [deg]	$10^3\times$CP2 [deg]	$10^6\times$CP3 [rad/sec]	$10^6\times$CP4 [rad/sec]	$10^2\times$CP5 [N-m]	CP6 [deg]	$10^3\times$CP7 [rad/sec]
Ba	0.12	0.70	1.12	3.96	106	27	120
BaF2	136	34	12	148	164	27	119
BaF4	151	167	85	1006	164	27	113
BaF6	162	93	52	463	275	37	152

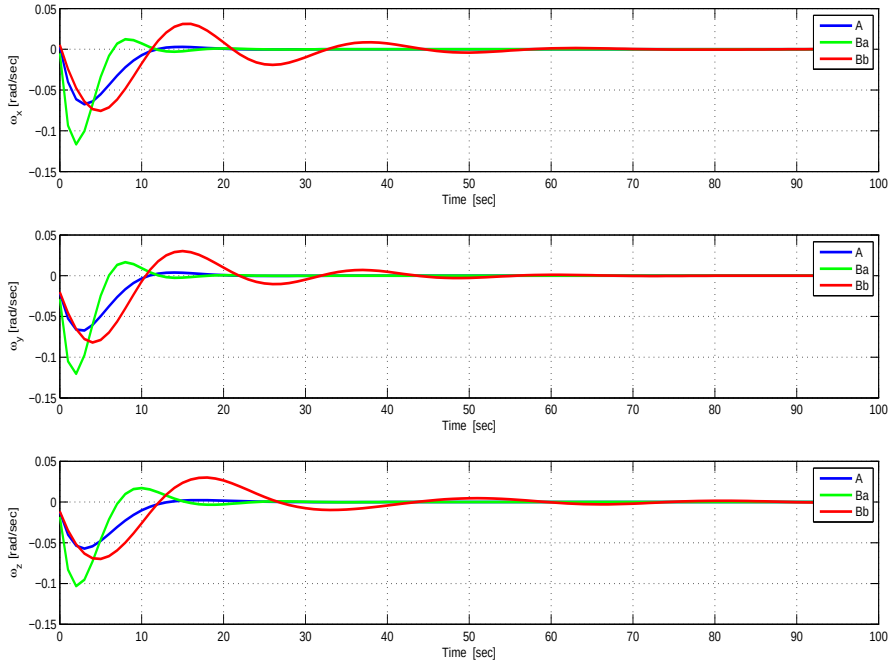

Figure 1: Time histories of the angular rates using single-loop and dual-loop SDRE controller

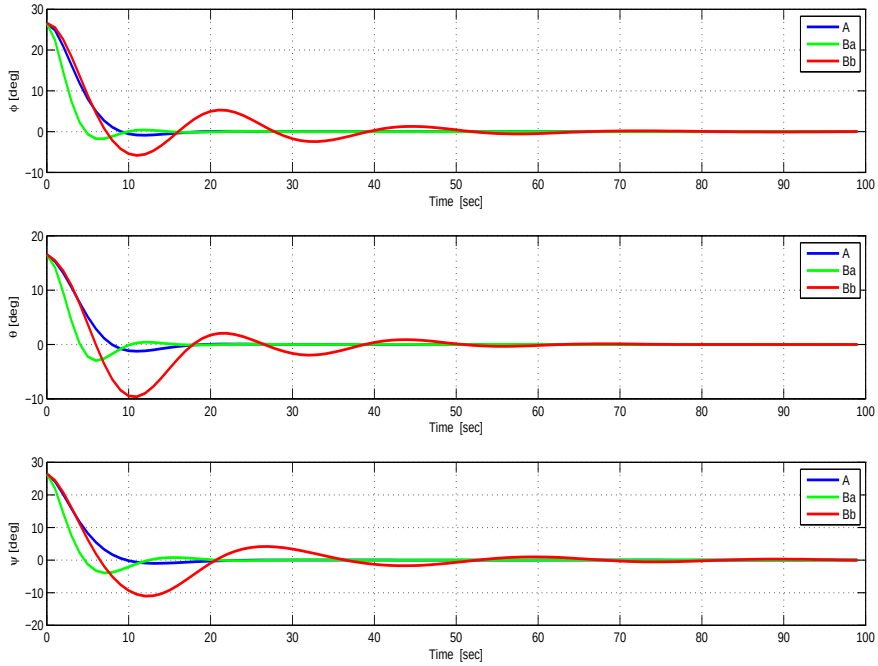

Figure 2: Time histories of the angular tracking errors using single-loop and dual-loop SDRE controller

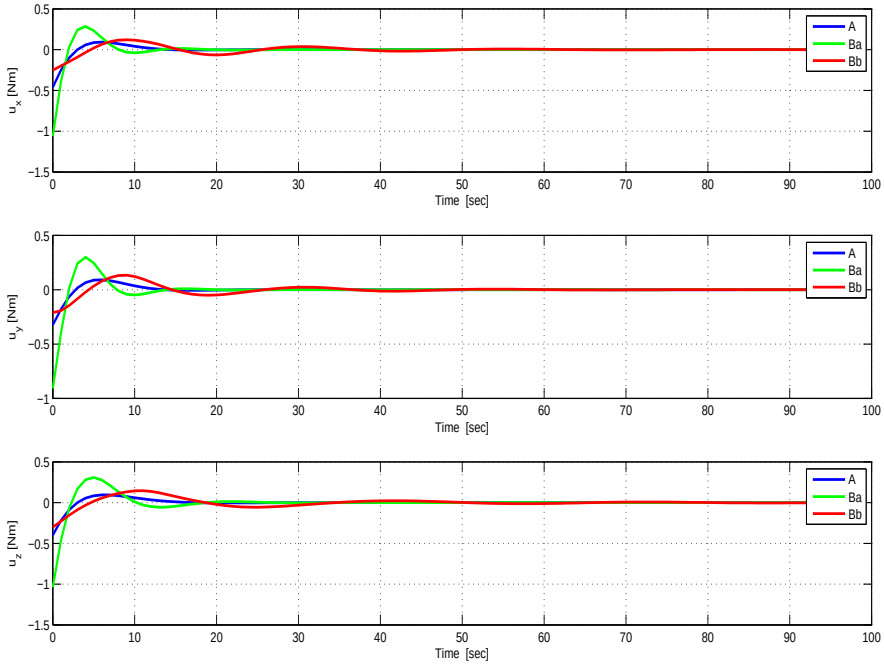

Figure 3: Time histories of the torque components using single-loop and dual-loop SDRE controller

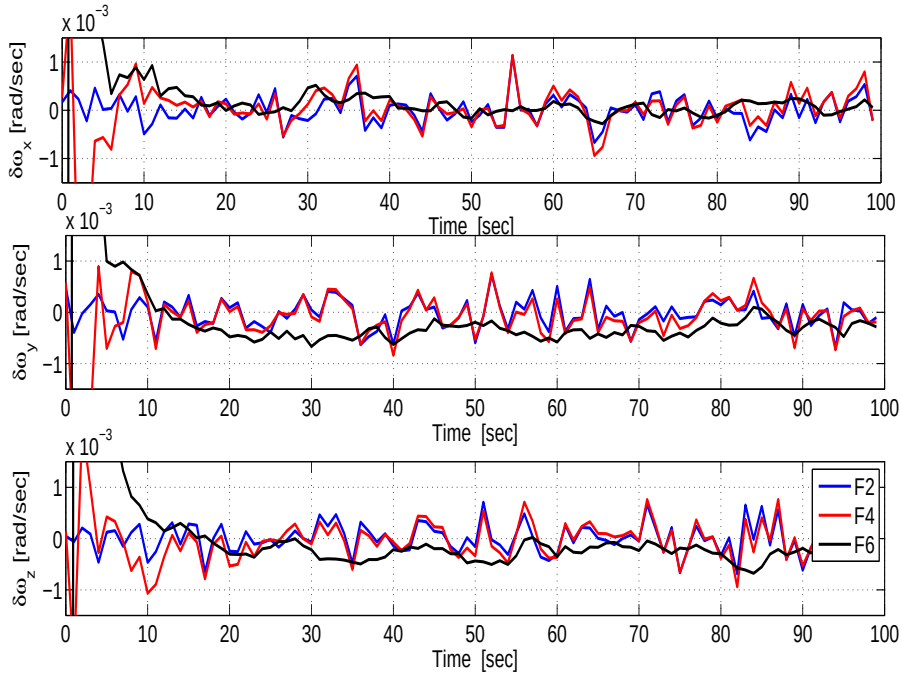

Figure 4: Time histories of the angular rates estimation errors for filters F2, F4, and F6. Single run. Control-free.

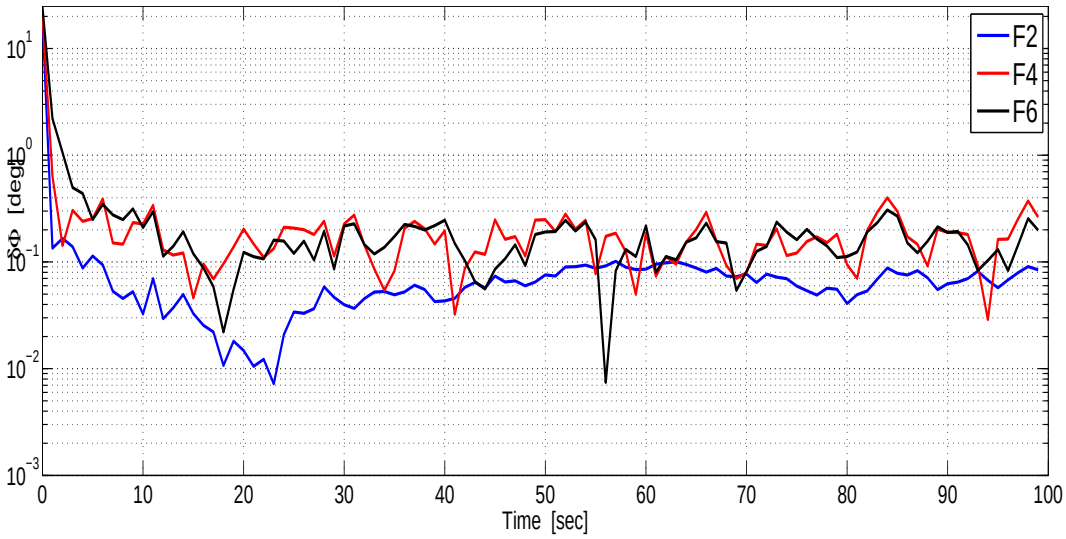

Figure 5: Time histories of the angular estimation error for filters F2, F4, and F6. Single run. Control-free.

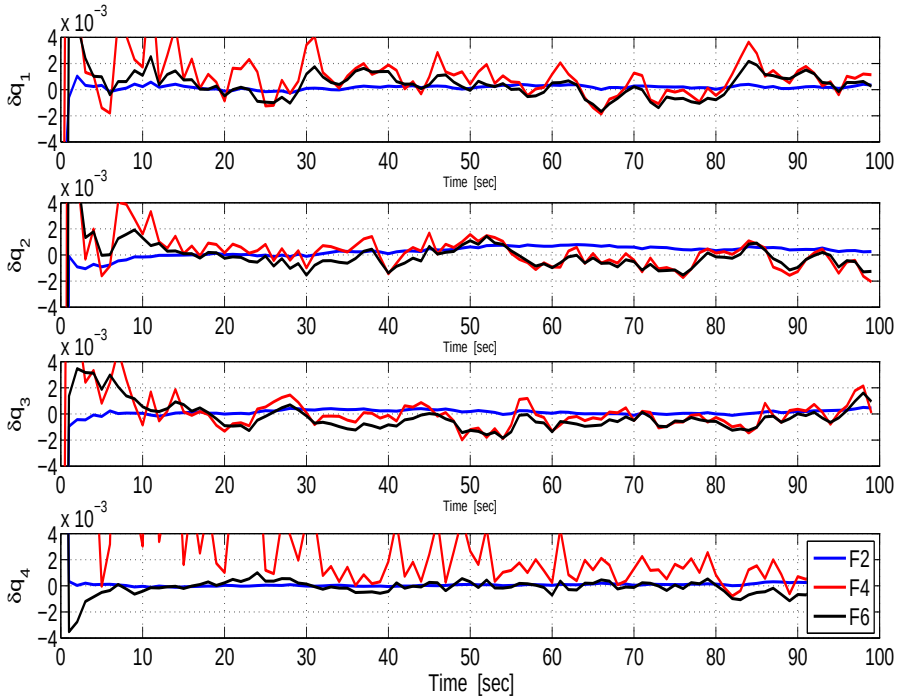

Figure 6: Time histories of the quaternion estimation error components for filters F2, F4, and F6. Single run. Control-free.

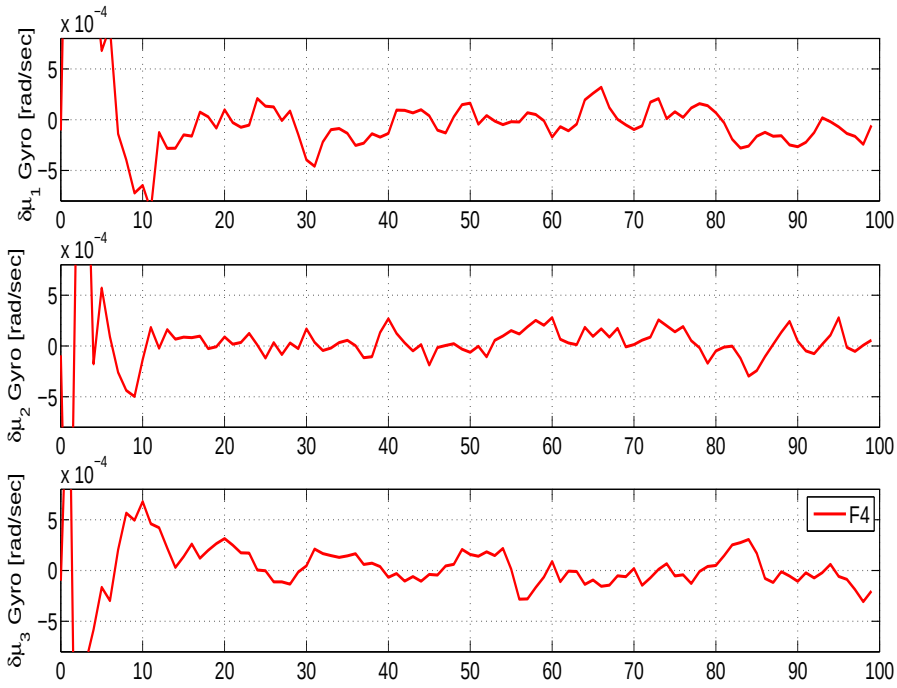

Figure 7: Time histories of the gyro drift estimation error components for filter F4. Single run. Control-free.

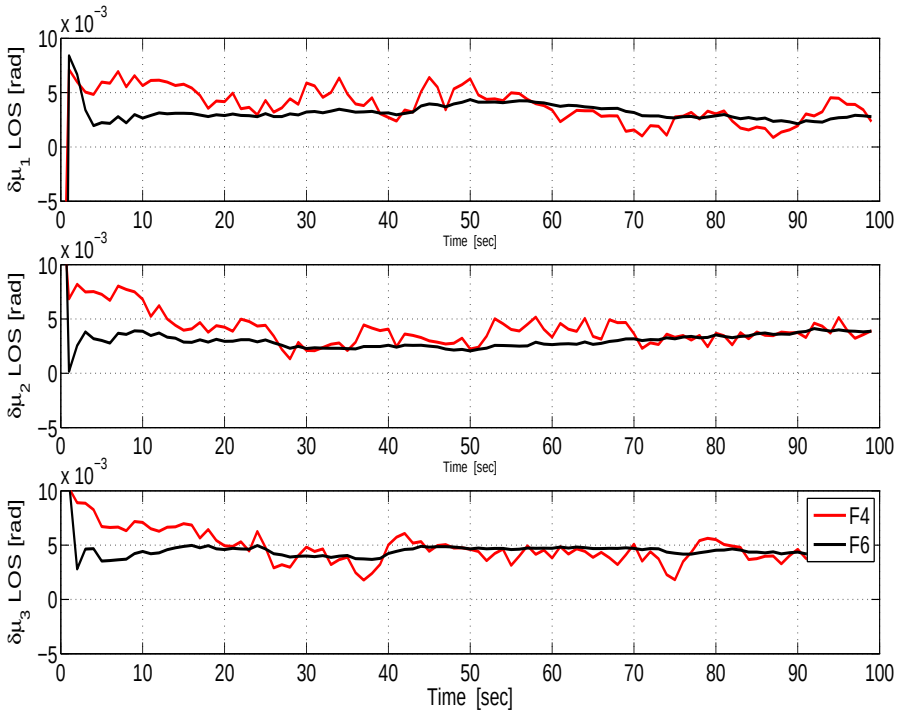

Figure 8: Time histories of the line-of-sight bias estimation error components for filters F4 and F6. Single run. Control-free.

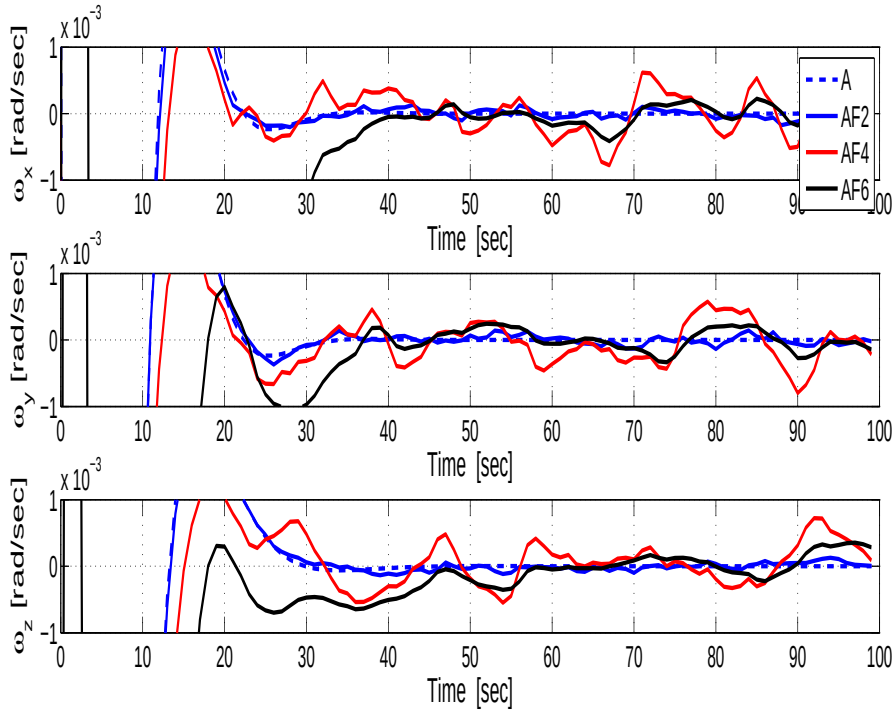

Figure 9: Time histories of the angular rates using the single-loop controllers with various filters.

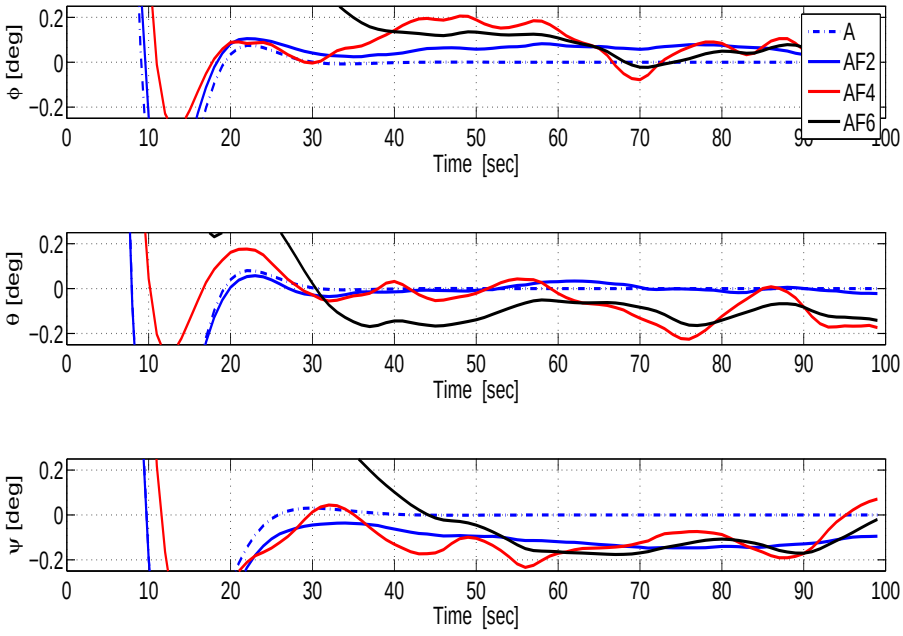

Figure 10: Time histories of the Euler angles using the single-loop controllers with various filters.

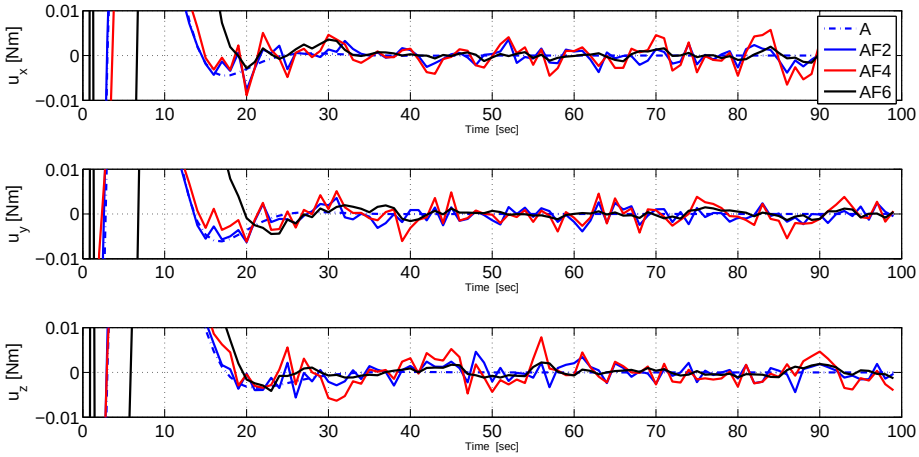

Figure 11: Time histories of the control torques using the single-loop controllers with various filters.

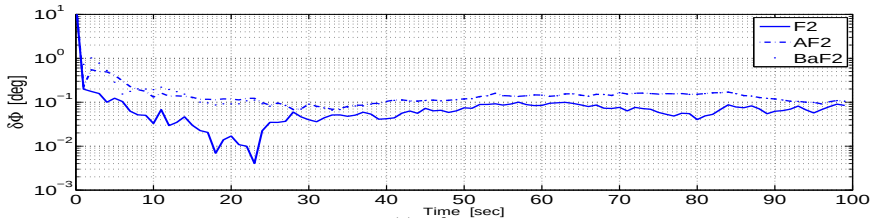

(a) Filter F2

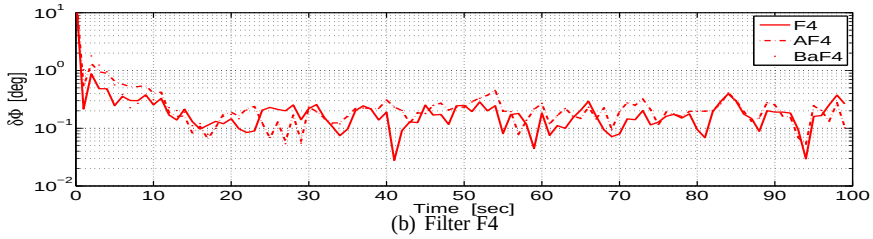

(b) Filter F4

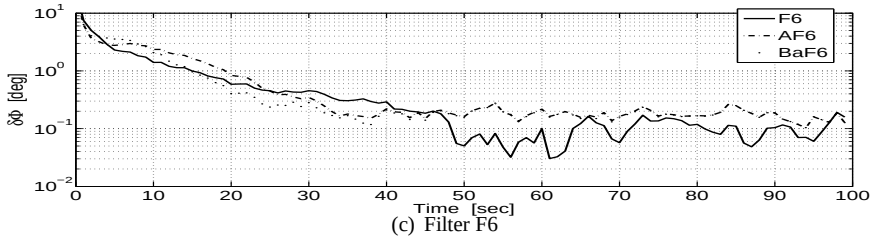

(c) Filter F6

Figure 12: Time histories of the angular estimation error in F2, F4, and F6, without control, with single-loop control A, and with dual-loop control Ba.